GA–A22982

EXPERIMENTAL TESTS OF TRANSPORT MODELS USING MODULATED ECH

by

J.C. DeBOO, J.E. KINSEY, R. BRAVENEC, E. FREDRICKSON,
C.M. GREENFIELD, Y.R. LIN-LIU, J. LOHR, T.C. LUCE, G.R. McKEE,
R. PRATER, C.L. RETTIG, D.P. SCHISSEL, G.M. STAEBLER,
and R.E. WALTZ

DECEMBER 1998

DISCLAIMER

GA–A22982

EXPERIMENTAL TESTS OF TRANSPORT MODELS USING MODULATED ECH

by
J.C. DeBOO, J.E. KINSEY,* R. BRAVENEC,† E. FREDRICKSON,‡
C.M. GREENFIELD, Y.R. LIN-LIU, J. LOHR, T.C. LUCE, G.R. McKEE,◊
R. PRATER, C.L. RETTIG,△ D.P. SCHISSEL, G.M. STAEBLER,
and R.E. WALTZ

This is a preprint of a paper to be presented at the 17th International Atomic Energy Agency Fusion Energy Conference, October 19–24, 1998, Yokohama, Japan, and to be published in *Special Issue of Nuclear Fusion.*

*Oak Ridge Associated Universities
†University of Texas at Austin
‡Princeton Plasmas Physics Laboratory
◊University of Wisconsin-Madison
△University of California, Los Angeles

Work supported by
the U.S. Department of Energy
under Contracts DE-AC03-89ER51114, DE-AC02-76CH03073,
and Grants DE-FG05-96ER54346, DE-FG02-92ER54139,
and DE-FG03-86ER53225

GA PROJECT 3466
DECEMBER 1998

ABSTRACT

Both the dynamic and equilibrium thermal responses of an L–mode plasma to repetitive ECH heat pulses were measured and compared to predictions from several thermal transport models. While no model consistently agreed with all observations, the GLF23 model was most consistent with the perturbed electron and ion temperature responses for one of the cases studied which may indicate a key role played by electron modes in the core of these discharges. Generally, the IIF and MM models performed well for the perturbed electron response while the GLF23 and IFS/PPPL models agreed with the perturbed ion response for all three cases studied. No single model agreed well with the equilibrium temperature profiles measured.

1. INTRODUCTION

Simulations have shown that perturbative transport experiments, where the dynamic plasma response is probed, can provide a more sensitive test of transport models compared to a comparison of measured and simulated temperature profiles from a power balance analysis. A perturbation source that deposits heat locally into the plasma particle species under study is preferred. Experiments have been performed on the DIII–D tokamak using modulated ECH as the perturbative heat source with the resonance layer off axis. The electron and ion response to the perturbation is measured and the amplitude and phase of the perturbations and the unperturbed temperature profiles are compared to predictions from several transport models.

2. TARGET PLASMA

To avoid inherent plasma perturbations such as sawteeth and ELMs, an MHD quiescent discharge in an L–mode configuration, limited on the inside wall of the vacuum vessel (Fig. 1), was chosen as the target plasma with a plasma current of 0.8 MA and electron density of $2–2.5 \times 10^{19} m^{-3}$. Early in the discharge, 4 MW of neutral beam power was applied to produce a sawtooth-free period during which 1.1–1.3 MW of ECH was applied in 20 ms pulses every 40 ms (Fig. 2) for a duration of 1 s. From 60%–75% of the total ECH power applied was in the X–mode with the remainder of the power in the O–mode. The X–mode power is calculated to be strongly absorbed during the first pass through the ECH resonance layer. Since the single pass absorption of the O–mode is low and the vessel walls are good reflectors, in the following simulation studies the O–mode power was assumed to be uniformly distributed along the vertical ECH resonance line through the plasma (Fig. 1). The ECH power was directed into the vessel so as to have the first pass absorption near the midplane of the vessel, which meant that the O–mode power was deposited no closer to the center of the plasma than the X–mode power. This was a necessary arrangement since the focus of the experiment was on the propagation from the off-axis deposition toward the plasma center. A toroidal field of 1.67 T resulted in second harmonic ECH power absorption (f_o = 110 GHz) at a normalized plasma radius ρ_{ECH} = 0.24–0.32. In order to probe more of the plasma two additional cases with ECH resonant layers at ρ_{ECH} = 0.4 and 0.5 were obtained by varying the launch angle of the ECH power and the toroidal field. The peak in the calculated ECH deposition profile is in reasonably good agreement with the spatial location of the peak change in the measured electron temperature produced by the ECH pulse for the ρ_{ECH} = 0.3 case. A similar comparison was not possible for the other two cases studied due to the limitation in spatial coverage, $\rho \leq 0.4$ for $B_T \leq 1.67$ T, of the electron cyclotron emission, ECE, system used to measure the electron temperature perturbations. Full spatial coverage of the electron temperature profile at discrete 6 ms time intervals was obtained from the combination of Thomson scattering and ECE measurements and full spatial coverage of the ion temperature profile and perturbations was obtained from charge exchange recombination, CER, measurements integrated over 4 ms intervals synchronized with the leading edge of the ECH pulse.

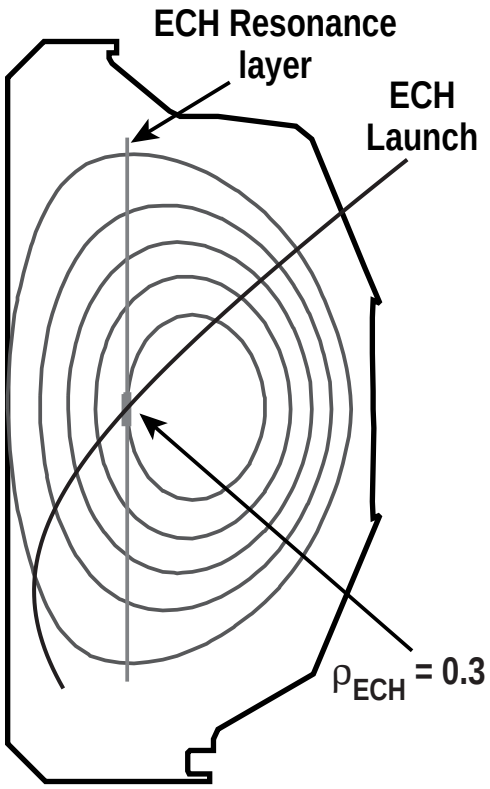

FIG. 1. Equilibrium flux plot of L–mode discharge. The first pass ECH absorption region is near the midplane of the vessel. Cases with ρ_{ECH} = 0.3, 0.4 and 0.5 were studied.

The unperturbed profiles for each of the three deposition locations were very similar with the ρ_{ECH} = 0.3 case having a slightly lower density which resulted in somewhat more peaked temperature and toroidal rotation profiles shown in Fig. 2. Plasma impurity content was dominated by carbon, resulting in Z_{eff} = 2 in the plasma core. The ratio of T_i/T_e is near one over the ECH resonance region for each of the cases studied. A ratio near one is at the marginal stability threshold for ion temperature gradient and electron temperature gradient turbulent drift wave modes. The impact of these modes on the experimental results are discussed in Section 4.

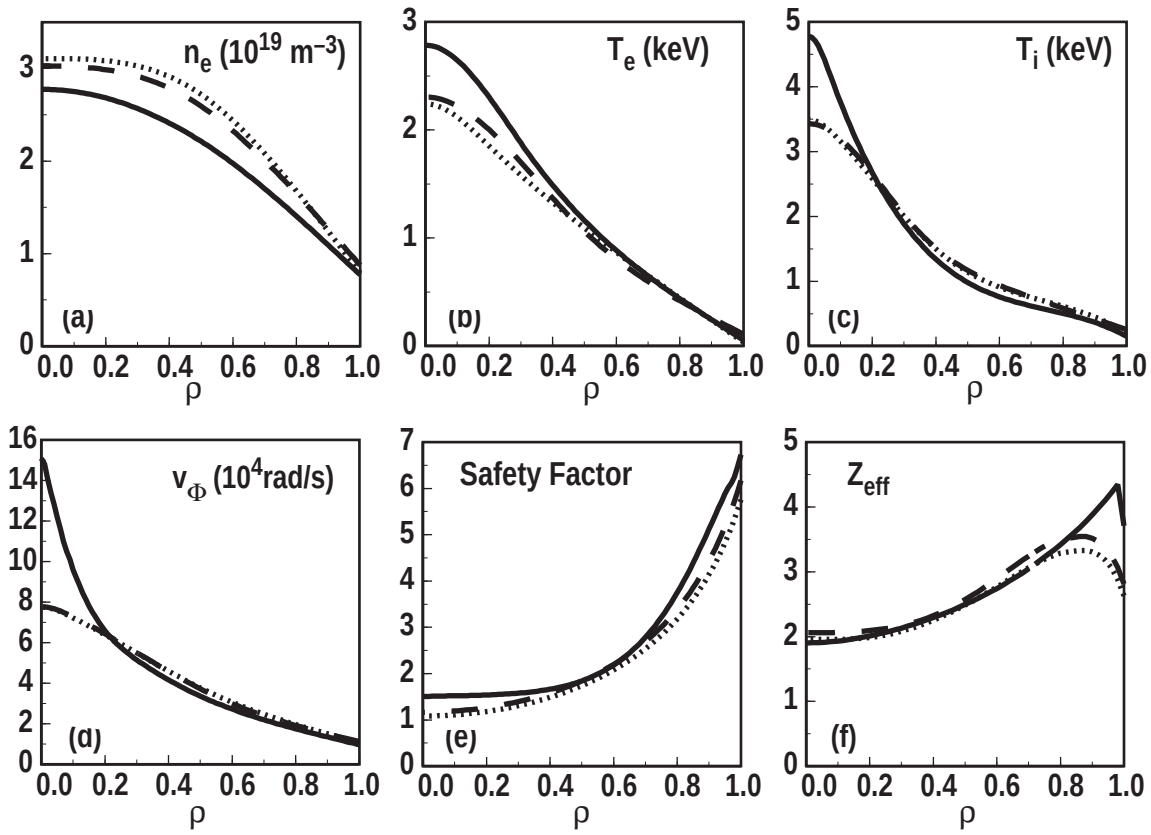

FIG. 2. Profiles of density (a), electron (b), and ion (c) temperature, toroidal rotation velocity (d), safety factor (e) and effective charge (f) for the three cases studied at ρ_{ECH} = 0.3 (solid line), 0.4 (dashed line) and 0.5 (dotted line).

3. PLASMA RESPONSE TO ECH

The ECH heat pulse produced peak-to-peak perturbations up to $\delta T_e \sim 200$ eV at the resonant layer for the case with $\rho_{ECH} = 0.3$ (Fig. 3). Smaller amplitude perturbations were produced for the other two cases since the local ECH power density decreased as the absorption volume increased at larger plasma radii. The electron perturbation pulse shape δT_e at $\rho = 0.3$ in Fig. 3 is consistent with integration of the applied heat pulse with some deviation from a linear rise due to transport during the heat pulse. The thermal energy confinement time for these discharges is 30–45 ms. The electron perturbation rapidly propagated to the plasma core with little phase shift while the amplitude was reduced to ~ 30 eV. The time averaging properties of Fourier analysis were employed to more clearly observe perturbations in the ion temperature. Results of this analysis showed that the ion temperature decreased in response to the electron heat pulse and the amplitude of δT_i increased as the perturbations propagated to the plasma core, in contrast to a decrease in δT_e, reaching peak-to-peak values up to ~ 200 eV for the case with $\rho_{ECH} = 0.3$. The high quality of the CER system allowed observation of changes in T_i as low as 2%. The ion temperature response at the resonant layer is ~180° out of phase with the electron response (Fig. 5) and also rapidly propagated to the plasma core, maintaining its out of phase relation to δT_e. It is important to note that the time scale for collisional transfer of energy between the perturbed electrons and background ions is several hundred milliseconds, long compared to the ECH modulation period, and hence changes in the ion temperature occur due to changes in the ion thermal diffusivity rather than changes in source or sink terms of the ion power balance. Power balance in these discharges is achieved by each species predominantly conducting away the neutral beam and average ECH power deposited.

It is interesting to note that the amplitude of density fluctuations was modulated by the ECH pulses. Measurements were taken at low k, below 3 cm^{-1}, with a beam emission spectroscopy (BES) diagnostic [1] and at higher k, near 12 cm^{-1} with a far infrared (FIR) scattering diagnostic [2]. For a discharge with $\rho_{ECH} = 0.7$, the amplitude of fluctuations measured by the BES system at $\rho = 0.55$ exhibited a 15% peak-to-peak modulation in phase with the ECH pulses (Fig. 4) while outside of ρ_{ECH} little or no modulation was observed. Modulation of the fluctuation amplitude at $\rho = 0.7$ with heating at smaller values of ρ_{ECH} was not observed, possibly due to smaller δT_e values produced at $\rho = 0.7$. The poloidal velocity of these fluctuations was modulated out of phase with the ECH pulses. This observation is consistent with previous experiments where application of ECH produced a slowing of plasma toroidal rotation and a reduction in radial electric field E_r since the poloidal velocity of the fluctuations is proportional to E_r in the absence of large diamagnetic flows [3], as expected for these discharges.

Modulation of larger k fluctuations was not observed with the FIR system. Preliminary results of work to model this turbulent fluctuation behavior have been reported elsewhere [4].

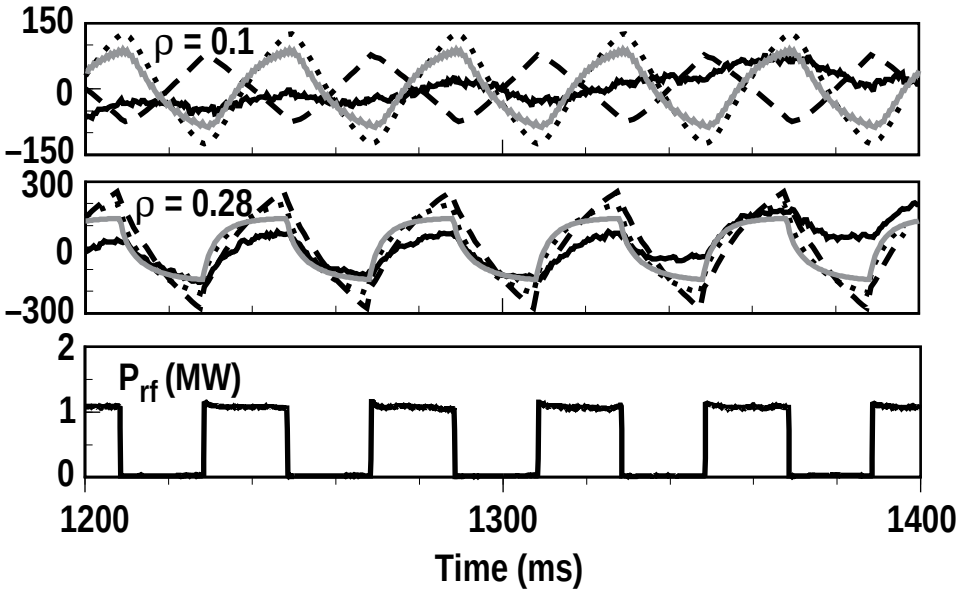

FIG. 3. Perturbed electron temperature, δT_e(eV), at ρ = 0.3 and ρ = 0.1 for measured data (solid, black lines), and simulated data from the IFS/PPPL model (dashed lines), IIF model (dotted lines), and GLF23 model (solid, grey lines).

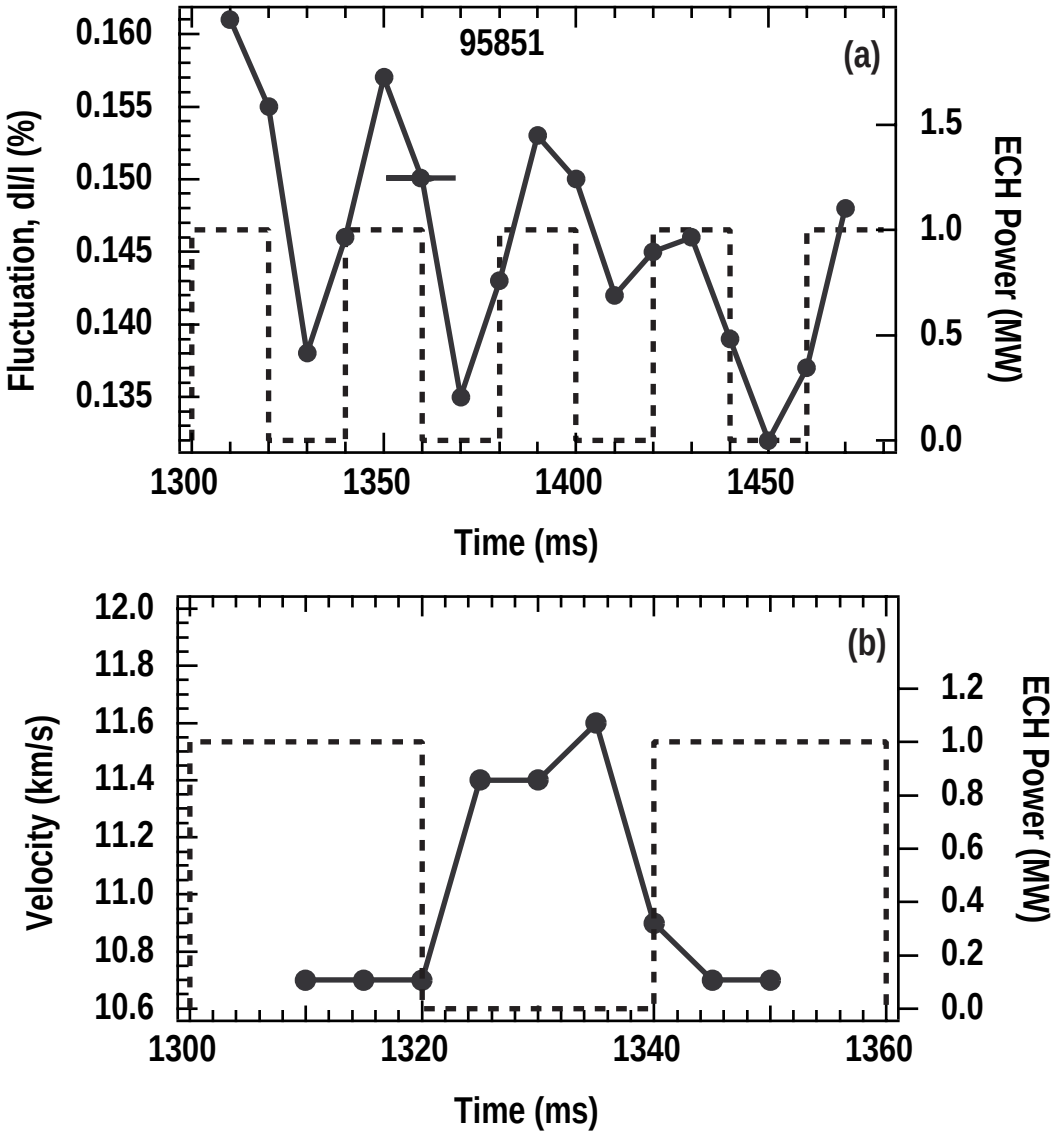

FIG. 4. Beam emission spectroscopy (BES) measurements of (a) amplitude of low k density fluctuations modulated in phase with the ECH pulse and (b) poloidal velocity of fluctuations modulated out of phase with the ECH pulse.

4. COMPARISON TO MODEL SIMULATIONS

Several theoretical and empirical models for describing electron and ion thermal transport have been examined. Two models which represent extremes in stiffness, a strong dependence on temperature gradients, are the IFS/PPPL model [5] based on ion temperature gradient (ITG) mode turbulence which depends sensitively on a critical temperature gradient and the Itoh-Itoh-Fukayama (IIF) model [6] based on current diffusive ballooning mode theory which has no critical temperature gradient dependence. The GLF23 model [7] contains essentially the same ITG physics model as does the IFS/PPPL model plus electron temperature gradient (ETG) modes and trapped electron (TEM) modes. The Multi-Mode (MM) model [6] also contains ITG and TEM modes but has no ETG modes and includes drift-resistive and kinetic ballooning modes. Simulations of the electron and ion temperature profile response to the ECH perturbative heating were performed with these models using a time-dependent transport code, MLT. Only thermal heat transport was considered and the temperature profile boundary conditions were taken from experimental measurements at $\rho = 0.9$. The electron density profile was held fixed at the steady-state experimentally measured level. The simulations were progressed in time until the predicted oscillatory perturbations about an equilibrium value were clearly determined. Fourier analysis was then applied to the prediction from each model and compared to the fourier analysis at the fundamental frequency of the electron and ion temperatures experimentally measured across the plasma. Fourier analysis significantly enhances the visibility of small amplitude perturbations immersed in a noisy or large amplitude background and was particularly necessary to clearly discern the experimental δT_i perturbations.

The ITG-based models agree with the electron and ion temperature profile response at the ECH resonance layer. For these models, the T_i response is largely determined by the effect of the T_i/T_e ratio on the ITG mode threshold. As the electrons are heated at ρ_{ECH}, T_i/T_e decreases which, if the plasma is near the marginal stability limit as was indicated in the previous section, destabilizes the ITG modes and thereby increases the ion transport at that location. This behavior is consistent with the decrease in T_i observed in response to the electron heat pulse and with the increased density fluctuations at low k observed with BES.

The Fourier amplitude of δT_e decreases while δT_i increases as it propagates toward the plasma core (Fig. 5). Each of the models was capable of reproducing this general trend. The models containing ITG modes most closely reproduced the amplitudes of δT_i. There is considerable disagreement between most model predictions of the amplitude of δT_e and measurements at the plasma center $\rho \leq 0.1$. However, it should be noted that in this region of the

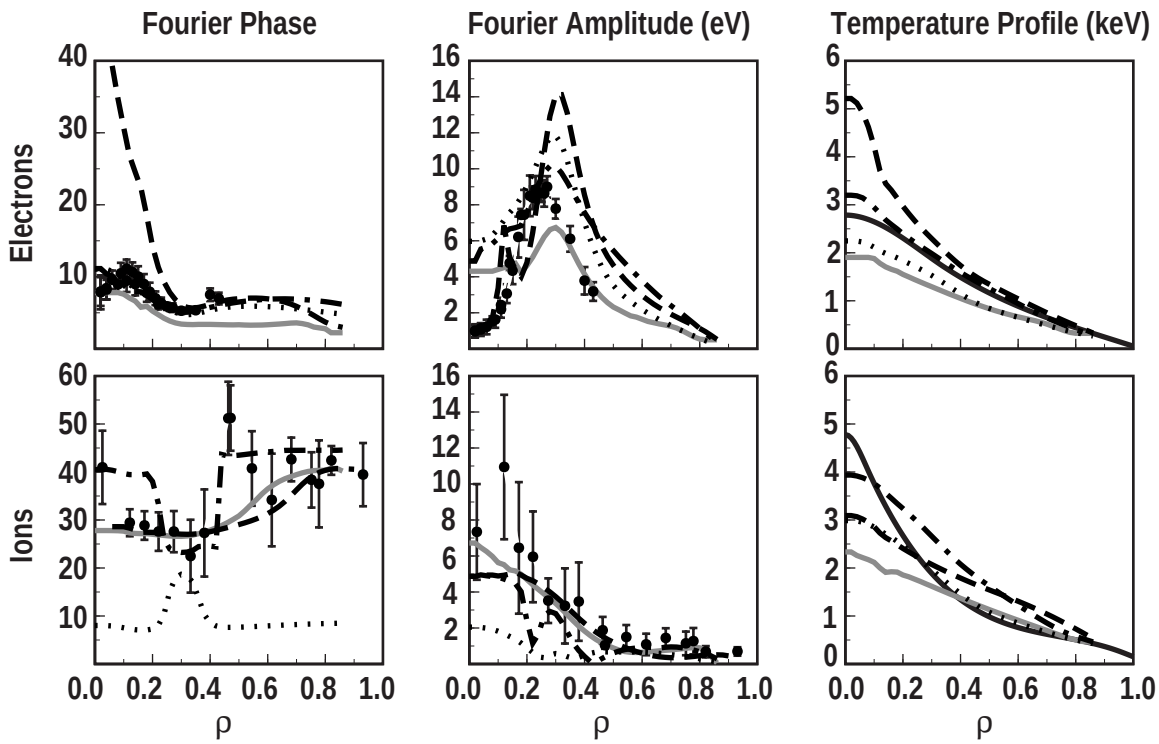

FIG. 5. Fourier analysis of phase and amplitude for δT_e and δT_i, T_e and T_i for measured data (circles and solid black lines), IFS/PPPL model (dashed lines), IIF model (dotted lines), MM model (dot-dashed lines), and GLF23 model (solid, grey lines) for the case with $\rho_{ECH} = 0.3$.

plasma the temperature gradients are below the critical temperature gradients for the ITG based models and therefore the measurements in the plasma core are being compared with underlying neoclassical trasnport. Hence, the comparison between models and measurments is focused in the region $0.1 \le \rho \le \rho_{ECH}$.

The predicted phase of δT_e and δT_i in the plasma core proved to be the most sensitive test for differentiating between the models. The general areas of agreement and disagreement between each of the models and the experimental results that are displayed in Fig. 5 for the case with $\rho_{ECH} = 0.3$ are also observed for the other two cases studied at $\rho_{ECH} = 0.4$ and 0.5 except for the agreement between the electron phase measured and the GLF23 model prediction. Only the GLF23 model is in reasonable agreement with the phase behavior of both δT_e and δT_i for the $\rho_{ECH} = 0.3$ case. Agreement with electrons is poorer for the other cases studied; predicted phase shifts are smaller than measured in the core. The IFS/PPPL model describes the ion phase well however it incorrectly predicts a ~180° phase shift in δT_e as it propagates inward from $\rho = 0.3$ to $\rho = 0.1$ whereas the experimental result exhibits only a small phase shift. The MM model has just the opposite problem; it describes the electron phase well but incorrectly predicts a ~180° phase shift in δT_i at $\rho = 0.2$ This abrupt change in phase is associated with an inversion in the sign of

the amplitude response so that at $\rho \leq 0.2$ the ion temperature is predicted to increase rather than decrease with the electron heat pulse. This phase change is associated with an abrupt change from the TEM mode calculated to be most unstable in the region where the ECH is absorbed to the ITG mode dominating closer to the plasma core. Ion phase shifts of ~180° are also observed and predicted by all of the ITG based models for $\rho \geq \rho_{ECH}$. Although shown for completeness, less emphasis is placed on the measurements and predictions at radii larger than ρ_{ECH} due to the difficulty stated earlier associated with the ECH O-mode power not being deposited locally. Finally, it is shown in Fig. 5 that the IIF model describes the observed electron phase behavior well but is rather discrepant with the ion behavior, incorrectly predicting that the ion pulse remains roughly in phase with the electron pulse near the plasma core.

The magnitude and shape of the unperturbed, equilibrium temperature profiles are generally not well described by any of the models. Differences between predicted and measured profiles described by an rms error typically exceed 20%. The shape of the T_e profile is reasonably well described by all but the IFS/PPPL model. The magnitude of T_e for GLF23 and IIF is somewhat low in the case shown in Fig. 3 and worse in other cases. The MM model predicts T_i well for the other cases studied but the shape for the case shown in Fig. 3 is not well matched.

5. DISCUSSION

The magnitude and shape of T_i in Fig. 5 is well described by the GLF23 and IIF models only for $\rho \geq 0.4$. The predicted central values of T_i and the entire T_e profile can be better matched with the GLF23 model by including E×B flow shear stabilization [9]. A comparison of GLF23 model predictions with and without E×B flow shear included is shown in Fig. 6. Although the agreement with central T_i values is improved, the mismatched shape of the T_i profile is not improved by including E×B flow shear. It is interesting to note that the inclusion of E×B flow shear predominately impacts the predicted equilibrium profiles without significantly changing the predicted perturbed amplitude or phase, indicating that the perturbed and equilibrium responses in at least this model are not necessarily closely coupled. Thus a complete test of the model requires both a time dependent and equilibrium power balance analysis. While including E×B flow shear in the IFS/PPPL model can improve the agreement with T_i in the core, predicted core T_e values become much too large. Since there are no ETG or TEM modes included in the IFS/PPPL model, the diffusivity drops to the neoclassical level when the ITG modes are stabilized.

There is experimental evidence supporting the inclusion of E×B flow shear effects for these discharges. The shearing rate, $\omega_{E\times B}$, normalized to the wave number k is compared with the normalized maximum linear growth rate for drift waves γ_{max}/k at $\rho = 0.3$, where the ECH is absorbed, in Fig. 7. The maximum growth rates were calculated with a linear gyro-kinetic stability code [10] using measured profiles. The comparison in Fig. 7 indicates that low k ITG and TEM modes may be marginally stabilized in these discharges since the growth rate and shearing rate are comparable while the ETG modes at larger k values remain unstable. ETG modes may be playing an important transport role in the plasma core, since the GLF23 model is the only model tested that includes ETG modes and is also the only model in reasonable agreement with both electron and ion perturbations for the case at $\rho_{ECH} = 0.3$.

The issue of the sensitivity of predicted perturbed results to the equilibrium temperature profiles has not been addressed in the analysis presented here. The extent to which the measured equilibrium T_e and T_i profiles are not reproduced by a given model may impact the model predictions for δT_e and δT_i. However, as mentioned above and shown in Fig. 6, comparison of the GLF23 analysis with and without E×B shear stabilization indicated that significantly different equilibrium profiles did not result in significant differences in predicted δT_e and δT_i values.

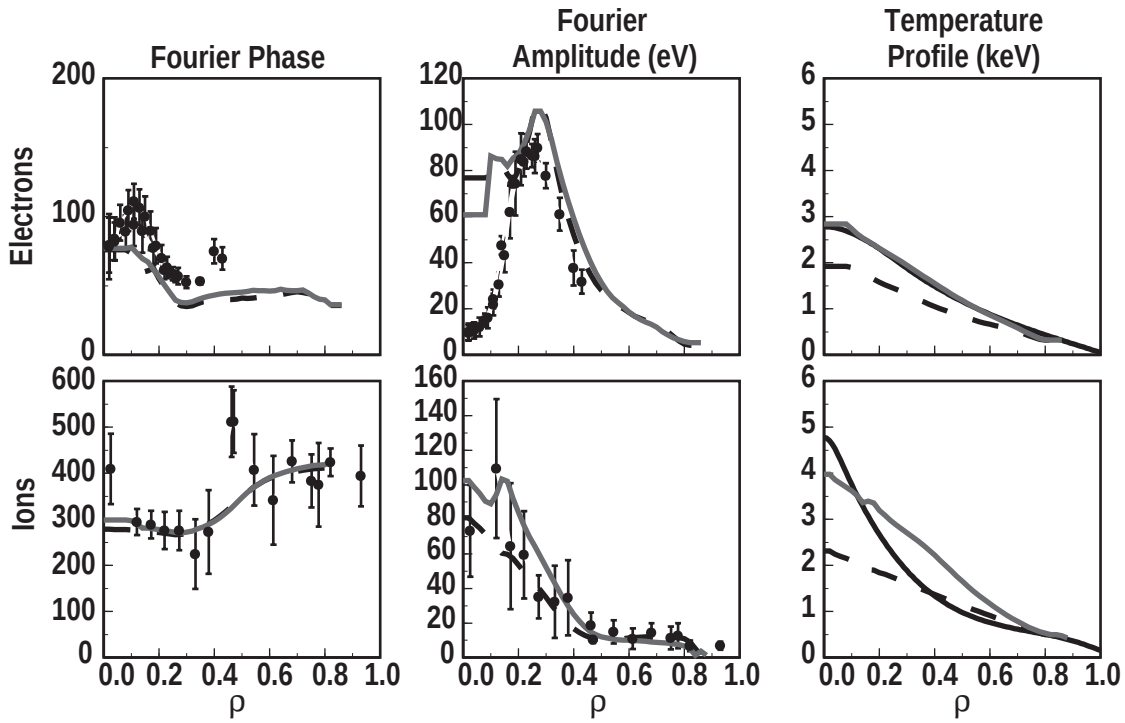

FIG. 6. Comparison of GLF23 model predictions with E×B shear included (solid grey line) and omitted (dashed line) for the case with ρ_{ECH} = 0.3. Measured data δT_e and δT_i (circles) and T_e and T_i profiles (black lines) are also shown.

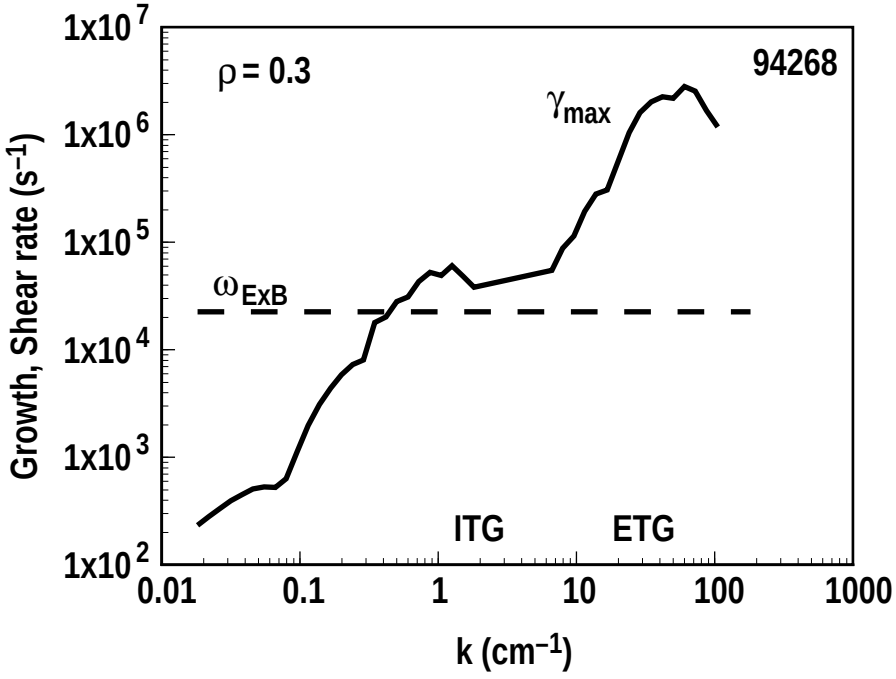

FIG. 7. Normalized E×B shearing rates (solid line) compared to normalized maximum linear growth rates (dashed line) for microturbulence at a normalized radius of 0.3 for the case with ρ_{ECH} = 0.3.

6. SUMMARY AND CONCLUSIONS

The overall observations indicate that the electron and ion responses to the ECH perturbation are out of phase with each other at the plasma core and at the resonance layer. Of the four models tested, the GLF23 model was closest to predicting this general characteristic at the plasma core which could indicate that electron modes, particularly ETG modes which are unique to the GLF23 model and calculated to be unstable, may be playing a key role in the heat transport near the core of these discharges. Since the electron and ion phase response to the heat pulse was very different it seems unlikely that a single fluid transport model will be capable of describing this behavior. The single fluid IIF model and the MM model described the electron behavior reasonably well in all cases studied but not the ion behavior while the IFS/PPPL and GLF23 models described the ion behavior reasonably well in all cases studied. Only the GLF23 model was in reasonable agreement with both electrons and ions for the case with $\rho_{ECH} = 0.3$. The overall results of these experiments remain a challenge for any one individual model to describe well and also demonstrate the usefulness of time dependent temperature perturbations for providing additional tests of transport models beyond a power balance analysis.

REFERENCES

[1] McKEE, G.R., *et al.*, "The Beam Emission Spectroscopy Diagnostic on the DIII–D Tokamak," to be published in Rev. Sci. Instrum. (1999).

[2] PHILIPONA, T., *et al.*, Rev. Sci. Instrum. **61**, 3007 (1990).

[3] McKee, G.R., *et al*. Bull. Am. Phys. Soc. **42**, 1921 (1997), to be submitted to Phys. Plasmas.

[4] BRAVENEC, R., *et al*., to be published in Proc. 25th EPS Conf. on Controlled Fusion and Plasma Physics, Prague, Czech Republic, 1998.

[5] KINSEY, J.E., *et al*., Phys. Plasmas **3**, 3344 (1996).

[6] ITOH, S.I., *et al*., Phys. Rev Lett. **72**, 1200 (1994).

[7] WALTZ, R.E., *et al*., Phys. Plasmas **4**, 2482 (1997).

[8] KINSEY, J.E., *et al*., Phys. Plasmas **3**, 3344 (1996).

[9] BURRELL, K.H., Phys. Plasmas 4 1499 (1997).

[10] KOTSCHENREUTHER, M., Bull. Am. Phys. Soc. **37**, 1432 (1992).

ACKNOWLEDGMENT

The authors gratefully acknowledge the contributions of the DIII–D Operations and RF groups in helping to carry out these experiments. We are also grateful to R. Groebner for his special analysis of the CER data. Work supported by U.S. Department of Energy under Contracts DE-AC03-89ER51114, DE-AC02-76CH03073 and Grant Nos. DE-FG05-96ER54346, DE-FG02-92ER54139, and DE-FG03-86ER53225.